The Plant Cell, Vol. 22: 755–771, March 2010, www.plantcell.org

Arabidopsis Homologs of Nucleus- and Phragmoplast-Localized Kinase 2 and 3 and Mitogen-Activated Protein Kinase 4 Are Essential for Microtubule Organization[W]

Martina Beck,[a,1] George Komis,[a,b,1] Jens Müller,[a] Diedrik Menzel,[a] and Jozef Šamaj[a,c,2]

[a] Institute of Cellular and Molecular Botany, University of Bonn, D-53115 Bonn, Germany
[b] Department of Botany, Faculty of Biology, University of Athens, GR-15784 Athens, Greece
[c] Centre of the Region Haná for Biotechnological and Agricultural Research, Faculty of Science, Palacký University, 783 01 Olomouc, Czech Republic

A double homozygous recessive mutant in the *Arabidopsis thaliana* homologs of nucleus- and phragmoplast-localized kinase 2 (*ANP2*) and 3 (*ANP3*) genes and a homozygous recessive mutant in the mitogen-activated protein kinase 4 (*MPK4*) gene of *Arabidopsis* exhibit deficiencies in the overall microtubule (MT) organization, which result in abnormal cell growth patterns, such as branching of root hairs and swelling of diffusely growing epidermal cells. Genetic, pharmacological, molecular, cytological, and biochemical analyses show that the major underlying mechanism for these phenotypes is excessive MT stabilization manifested in both mutants as heavy MT bundling, disorientation, and drug stability. The above defects in MAPK signaling result in the adverse regulation of members of the microtubule-associated protein (MAP65) protein family, including strongly diminished phosphorylation of MAP65-1. These data suggest that ANP2/ANP3, MPK4, and the microtubule-associated protein MAP65-1, a putative target of MPK4 signaling, are all essential for the proper organization of cortical microtubules in *Arabidopsis* epidermal cells.

INTRODUCTION

Regulation of plant growth and organ shape is tightly coupled to cell growth and cytomorphogenesis (Smith, 2001). Both functions are intimately associated with the tight regulation of microtubule (MT) organization and dynamics during diffuse and polar cell growth (Sieberer et al., 2005; Sedbrook and Kaloriti, 2008). MTs are steady state polymers of the α/β-tubulin dimer with an inherent capacity to self-organize into complex structures (Desai and Mitchison, 1997). Both MT assembly and dynamics are assisted by the coordinated action of MT-associated proteins (MAPs) and regulatory proteins that modulate either the affinity of MAPs for the MT surface (Cassimeris and Spittle, 2001), the rates of exchange of tubulin subunits (Akhmanova and Steinmetz, 2008), or the dynamic organization of large MT populations (Wasteneys, 2002; Sedbrook, 2004; Sedbrook and Kaloriti, 2008). The function of some of these MAPs is regulated by reversible phosphorylation (Sasabe et al., 2006; Smertenko et al., 2006; Wasteneys and Ambrose, 2009). So far, however, there is only limited information about the involvement of mitogen-activated protein kinase (MAPK) signaling in MT organization in plants (Šamaj et al., 2004; Sasabe and Machida, 2006; Smertenko et al., 2006; Walia et al., 2009). MT disruption by oryzalin activates heat shock–activated MAPK and stress-activated MAPK in alfalfa (*Medicago sativa*; Sangwan et al., 2002), suggesting a role for these MAPKs in MT dynamics. MMK3 from *M. sativa* is thought to be indispensable for spindle MT reorganization during mitosis (Bögre et al., 1999, 2000). To date, only one MAPK signaling pathway with implications in cytoskeletal organization has been largely resolved. This pathway is elemental for the progression of cytokinesis in tobacco (*Nicotiana tabacum*) and comprises of the NPK1-activating kinesin-like protein 1 (NACK1) and NACK2 (Ishikawa et al., 2002; Nishihama et al., 2002; Tanaka et al., 2004), the nucleus- and phragmoplast-localized protein kinase 1 (NPK1) (Nishihama and Machida, 2000, 2001; Nishihama et al., 2001; Soyano et al., 2002; Takahashi et al., 2004; Tanaka et al., 2004), the NQK1 MAPK kinase (MAPKK), and the NRK1 MAPK (NACK-PQR pathway; Takahashi et al., 2004). It is thought that the activated pathway ultimately targets the tobacco MAP65-1a and 1b isoforms to promote MT dynamics for the expansion of the phragmoplast. Thus far, *Arabidopsis thaliana* putative orthologs of every member of the above pathway have emerged. The *Arabidopsis* ANP family is putatively orthologous to NPK1 (Krysan et al., 2002), *Arabidopsis* MKK6 is a putative ortholog of NQK1 (Soyano et al., 2003; Menges et al., 2008), and *Arabidopsis* MPK13 is a putative ortholog of NRK1 and can be activated by *Arabidopsis* MKK6 (Melikant et al., 2004). The NACK1 and NACK2 activators of the NPK1 pathway are

[1] These authors contributed equally to this work.
[2] Address correspondence to jozef.samaj@uni-bonn.de.
The author responsible for distribution of materials integral to the findings presented in this article in accordance with the policy described in the Instructions for Authors (www.plantcell.org) is: Jozef Šamaj (jozef.samaj@uni-bonn.de).
[W] Online version contains Web-only data.
www.plantcell.org/cgi/doi/10.1105/tpc.109.071746

homologous to the respective *Arabidopsis* genes *HINKEL* and *STUD/TETRASPORE* (Strompen et al., 2002; Yang et al., 2003; Tanaka et al., 2004). Here, we present data on postcytokinetic epidermal phenotypes and the regulation of cortical MT organization in *anp2 anp3* and *mpk4* knockout mutants. These results indicate that ANP2/ANP3, MPK4, and the MT-associated protein MAP65-1 are involved in MT-dependent cell growth mechanisms in *Arabidopsis*.

RESULTS

anp2 anp3 and *mpk4* Mutants Show Similar Root Hair Phenotypes and Radial Root Expansion

To characterize phenotypic aberrations, homozygous seedlings of *anp2 anp3* and *mpk4* mutants, were screened 4 to 6 d after germination. The dwarf phenotype of the *mpk4* mutant grown in soil as well as cytokinetic defects in leaf epidermal cells of this mutant (see Supplemental Figure 1 online) were consistent with similar phenotypes previously observed in the *anp2 anp3* mutant (Krysan et al., 2002). Both these mutants showed retarded growth and significantly shorter roots compared with wild-type seedlings (see Supplemental Figures 2A and 2B online). More detailed microscopy examinations of roots in both mutants showed double- or multiple-branched root hairs compared with the respective wild types (Figures 1B 1D, 1G, and 1I). It must be noted that most of the root hairs observed in the *mpk4* mutant displayed highly abnormal forms, including double or triple branches, a thickened root hair base, or an abnormal tube form (Figures 1D and 1I, arrows). Time-lapse images of root hair growth in the *anp2 anp3* mutant showed the emergence of lateral root hair branches and ectopic root hairs (see Supplemental Figures 3A to 3G online). Likewise, ectopic root hairs were also present in the *mpk4* mutant (see Supplemental Figures 3H to 3J online). Further observations revealed other aberrations, not restricted to root hairs. In both mutants, root epidermal cells showed radial expansion (Figures 1E and 1J, arrowheads), indicating a defect in cortical MT regulation. Such irregularities were initially described for hypocotyl epidermal cells of the *anp2 anp3* mutant (Krysan et al., 2002). Here, we report that root epidermal cells of both investigated mutants also showed such aberrant cell forms. Moreover, mutant roots appeared radially swollen (cf. Figures 1C to 1E with Figures 1A and 1B and Figures 1H to 1J with Figures 1F and 1G), which indicates an overall disturbance in the uniaxial mode of diffuse cell growth.

To quantify these phenotypes, the numbers of normally growing root hairs versus branched or otherwise abnormal root hairs (swollen root hair base or aberrant tube form) from at least 30 individual plants were counted. Abnormally growing root hairs account for ~48% of all root hairs in the *anp2 anp3* double mutant and over 75% of those in the *mpk4* mutant (Figure 1K). Measurements of the root width at ~200 μm distance from the tip revealed that root diameter in the *anp2 anp3* and *mpk4* mutants was between 170 and 230 μm, which is significantly greater than the diameter of Wassilewskija (Ws) and Columbia-0 (Col-0) roots (120 to 130 μm; Figure 1L). Since the root phenotype of *mpk4* was more pronounced than that of *anp2 anp3*, we further characterized it by microscopy visualization using semithin sections. Cross-sectional analysis demonstrated bulging of root epidermal cells, but also a general disturbance of root architecture and loss of anisotropy in cortical and endodermal cells (see Supplemental Figure 4 online). Similar, albeit less pronounced, features were observed on sections prepared from embryos, hypocotyls, and inflorescence bolts of the *anp2 anp3* mutant (Krysan et al., 2002).

MPK4 Expression in Root Hairs

Analysis of the level of gene transcription in flowers, leaves, stems, and roots of *Arabidopsis* wild-type plants confirmed that *MPK4* transcripts are detectable in all of these organs (see Supplemental Figure 4A online). To investigate the expression pattern of *MPK4* at the tissue and cellular levels, experiments with β-glucuronidase (GUS) reporter gene constructs under the control of the *MPK4* promoter were performed. The expression pattern was analyzed in *ProMPK4:GUS* transgenic plants. GUS staining was found in root epidermal cells and root hairs, especially in the root hair formation zone (see Supplemental Figures 5B and 5C online). During root hair development, *MPK4* promoter activity was detectable in both root hair bulges and in young outgrowing root hairs (see Supplemental Figure 2C online). These expression data confirm *MPK4* expression in the root regions and cell types affected in the root phenotypes observed here and emphasize the role of MPK4 in root development, including development and growth of root hairs and epidermal cells.

MT Organization in *anp2 anp3* and *mpk4* Mutants

Both branched and/or ectopic root hairs (Bibikova et al., 1999; Bao et al., 2001; Sakai et al., 2008) as well as radial expansion of cells (Baskin et al., 1994; Whittington et al., 2001; Sugimoto et al., 2003; Collings et al., 2006; Gardiner et al., 2008) were closely related to defects in the MT cytoskeleton. These distinct root hair phenotypes and the disturbed cell expansion in both mutants suggest aberrant MT organization. The analysis of MT organization was initially conducted by whole-mount tubulin immunofluorescence labeling in roots (Müller et al., 2010) of both *anp2 anp3* and *mpk4* mutants and compared with labeling in their respective wild types. Cortical MTs appeared heavily bundled and showed random configurations in all swollen epidermal cells of both mutants within root meristem regions (cf. Figures 2A and 2B, and Figures 2C and 2D, respectively).

Subsequently, the in vivo organization of MTs was studied more thoroughly in all major organs of the *anp2 anp3* and *mpk4* plants and the respective wild types stably transformed with the *35S:GFP:MBD* (GFP for green fluorescent protein) MT reporter (Marc et al., 1998; Granger and Cyr, 2001; Müller et al, 2007). The cortical MTs in the epidermal cells of growing control (Ws and Col-0) root (Figures 3R and 3T) and hypocotyl (Figures 3C and 3G) were arranged in a parallel configuration, forming oblique to transverse arrays. By contrast, the cortical MTs of both mutants showed several similar aberrant features in nearly every tissue examined. In hypocotyl epidermal cells of both *anp2 anp3* (Figures 3B and 3D) and *mpk4* (Figures 3H and 3J) mutants, cortical MTs appeared disoriented, forming random net-like

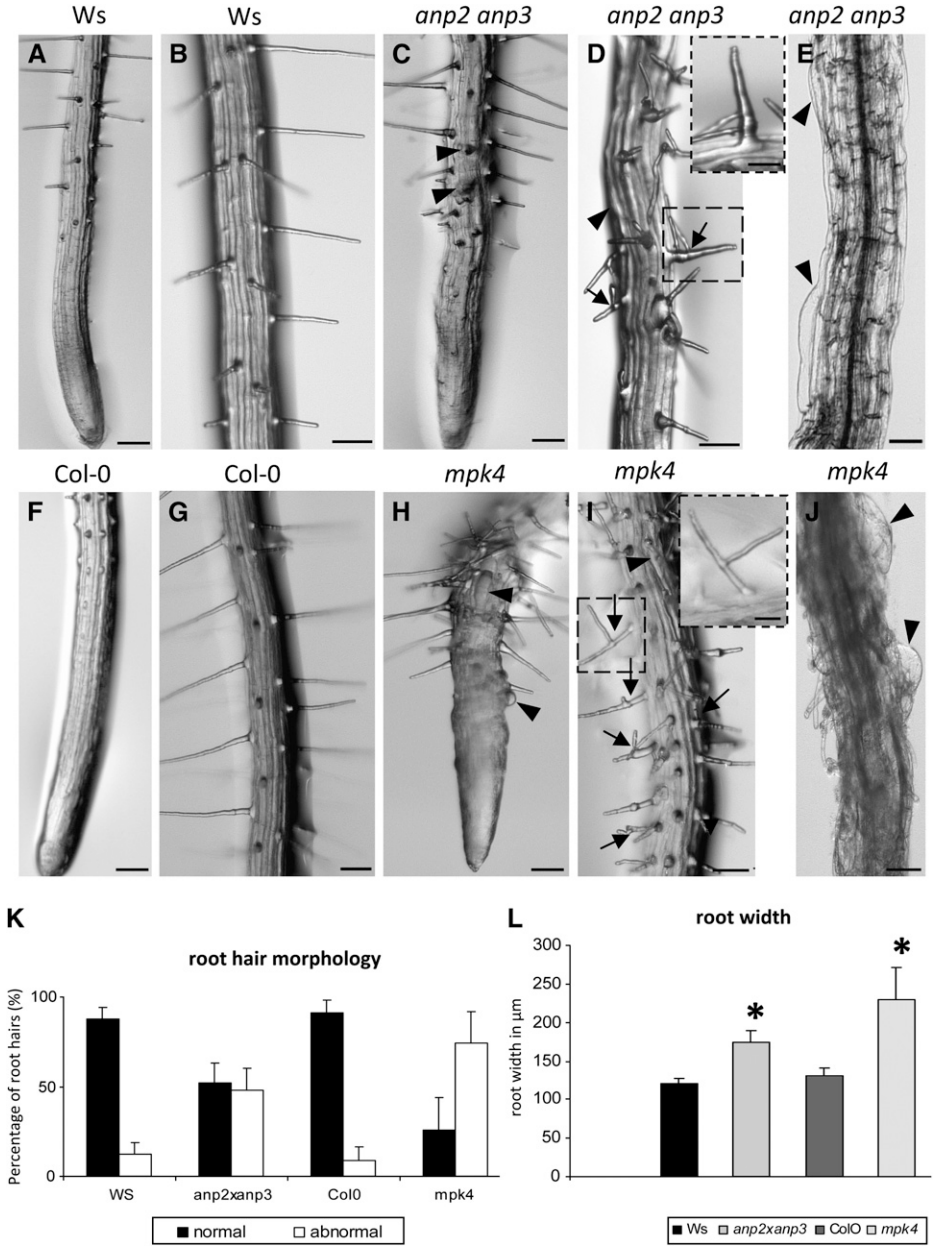

Figure 1. Root Phenotype Comparisons among Ws, *anp2 anp3*, Col-0, and *mpk4.*

(A) to **(E)** Roots of Ws plants showing smooth root outline and straight-growing root hairs (**[A]** and **[B]**). By contrast, roots of the *anp2 anp3* mutant (**[C]** and **[E]**) appear radially swollen with bulging epidermal cells (arrowheads) and bear branched root hairs (arrows). Inset in **(D)** shows detail on branched root hair in the indicated boxed area. Bars = 100 μm; 30 μm for the inset.

(F) to **(J)** Normal root morphology in the control (Col-0) plant (**[F]** and **[G]**) and highly abnormal root morphology of the *mpk4* mutant (**[H]** to **[J]**) showing radial swelling of epidermal cells (arrowheads) and branching of root hairs (arrows). Inset in **(I)** shows detail on branched root hair in the indicated box area. Bars = 100 μm; 30 μm for the inset.

(K) Graphic depiction of the percentage of branched or otherwise abnormal root hairs in *anp2 anp3* and *mpk4* seedlings compared with control Ws and Col-0 seedlings, respectively. Note that 76% of root hairs in *mpk4* seedlings and 48% of root hairs in *anp2 anp3* seedlings are branched and/or deformed. Only 9 and 11% of branched root hairs could be found in Col-0 and Ws control plants, respectively.

(L) Graphic depiction of root width in micrometers of *anp2 anp3* and *mpk4* seedlings compared with control Ws and Col-0 seedlings, respectively. Both mutants show increased root width, more strongly affected in the *mpk4* mutant. Values are for Ws, 122.09 μm ± 9 (SD); *anp2 anp3*, 173.53 μm ± 21.92 (SD); Col-0: 129.875 μm ± 12.38 (SD); and *mpk4*, 224 μm ± 42.77 (SD). Asterisks indicate statistically significant difference between mutants and corresponding controls as revealed by Student's *t* test ($P < 0.05$).

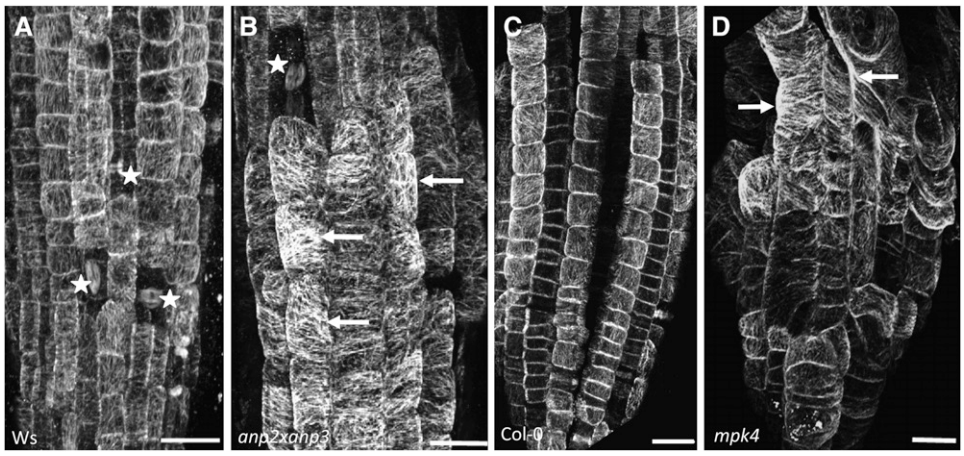

Figure 2. In Situ Localization of MTs in *anp2 anp3* and *mpk4* Mutants.

Immunofluorescence localization of MTs in roots of Ws **(A)**, *anp2 anp3* **(B)**, Col-0 **(C)**, and *mpk4* **(D)** plants. Arrows indicate examples of thick and deregulated MT bundles in both mutants. Asterisks denote mitotic cells. Bars = 10 μm

arrays at the cell cortex instead of parallel arrays. However, the most prominent feature was the large extent of bundling of cortical MTs in both mutants (cf. Figures 3C and 3G with Figures 3D and 3H). Similarly, cotyledon pavement cells of both *anp2 anp3* and *mpk4* showed a simpler cell shape and at the same time an increased bundling of cortical MTs (cf. Figures 3E and 3K with Figures 3F and 3L, respectively). The aberrant-branched and/or swollen root hairs of *anp2 anp3* and *mpk4* roots also had more prominent MT bundling compared with the respective wild-type plants (cf. Figures 3M and 3O with Figures 3N, 3P, and 3Q). Similarly to the hypocotyl epidermal cells, the root epidermal cells of both mutants showed a loss of parallel cortical MT organization accompanied by increased bundling (cf. Figures 3R and 3T with Figures 3S and 3U).

Cortical MTs of *anp2 anp3* and *mpk4* Show Increased Resistance to Oryzalin

A physiological consequence of MT bundling was a profound stability of MTs to MT-disrupting drugs in *anp2 anp3* and *mpk4* hypocotyl epidermal cells (Figure 4). In wild-type cells, either Ws or Col-0, a treatment with 5 μM oryzalin for 15 to 30 min was sufficient to eliminate the vast majority of cortical MTs (Figure 4). By contrast, MTs in hypocotyl epidermal cells of *anp2 anp3* and *mpk4* were resistant to this concentration of oryzalin. After pretreatement of the wild types with the MAPKK inhibitor PD98059 (see below), cortical MTs in the hypocotyls were also resistant to oryzalin and stayed bundled, though randomly oriented, for at least 90 min (Figure 4, bottom panel). The resistance of cortical MTs appeared to correlate with the degree of bundling.

Association of MPK4 with MTs

The putative association of MPK4 with MTs was studied biochemically in postnuclear, organelle-depleted cell extracts supplemented with bovine brain MTs in the presence of taxol and GTP. MTs and the associated proteins were pelleted three times through a 20% glycerol cushion to eliminate nonspecific contaminants in the final MT pellet, which finally was studied by SDS-PAGE and immunoblot analysis using an antibody against MPK4. The MT pellet contained a prominent fraction of MPK4 (Figure 5), although there was still a substantial amount of MPK4 left in the supernatant. This suggests that not all of the MPK4 associates with MTs but that some also associates with other cellular compartments, as has been recently described for MPK6 (Müller et al., 2010). The addition of recombinant 6×His-tagged MAP65-1 did not significantly improve the yield of MPK4 in the MT pellet.

Effects of Specific MAPKK Inhibitor PD98059 on the Cortical MT Organization

To test whether the association of MPK4 with MTs has functional implications, we treated either Col-0 or Ws wild-type plants, stably transformed with the *35S:GFP:MBD* reporter for MTs, with the potent MAPKK inhibitor PD98059, which prevents the activation of MAPKs. The MPK4 activation induced by the osmotic stress following sorbitol treatment was abolished in the presence of PD98059 (see Supplemental Figure 6A online). Also, in root epidermal cells treated with PD98059, the cortical MTs became highly bundled in a time-dependent fashion (Figure 6).

Transmission Electron Microscopy Observations Reveal a Putative Mechanism Underlying MT Bundling in the *anp2 anp3* Mutant

Transmission electron microscopy (TEM) visualization of interphase cortical and endoplasmic MTs of control root and hypocotyl cells of the Ws wild type showed the occurrence of loose MT bundles with a spacing distance of ~25 nm (Figure 7A). Cortical MTs were sparsely arranged in the cortical cytoplasm and in most cases formed a single layer beneath the plasma

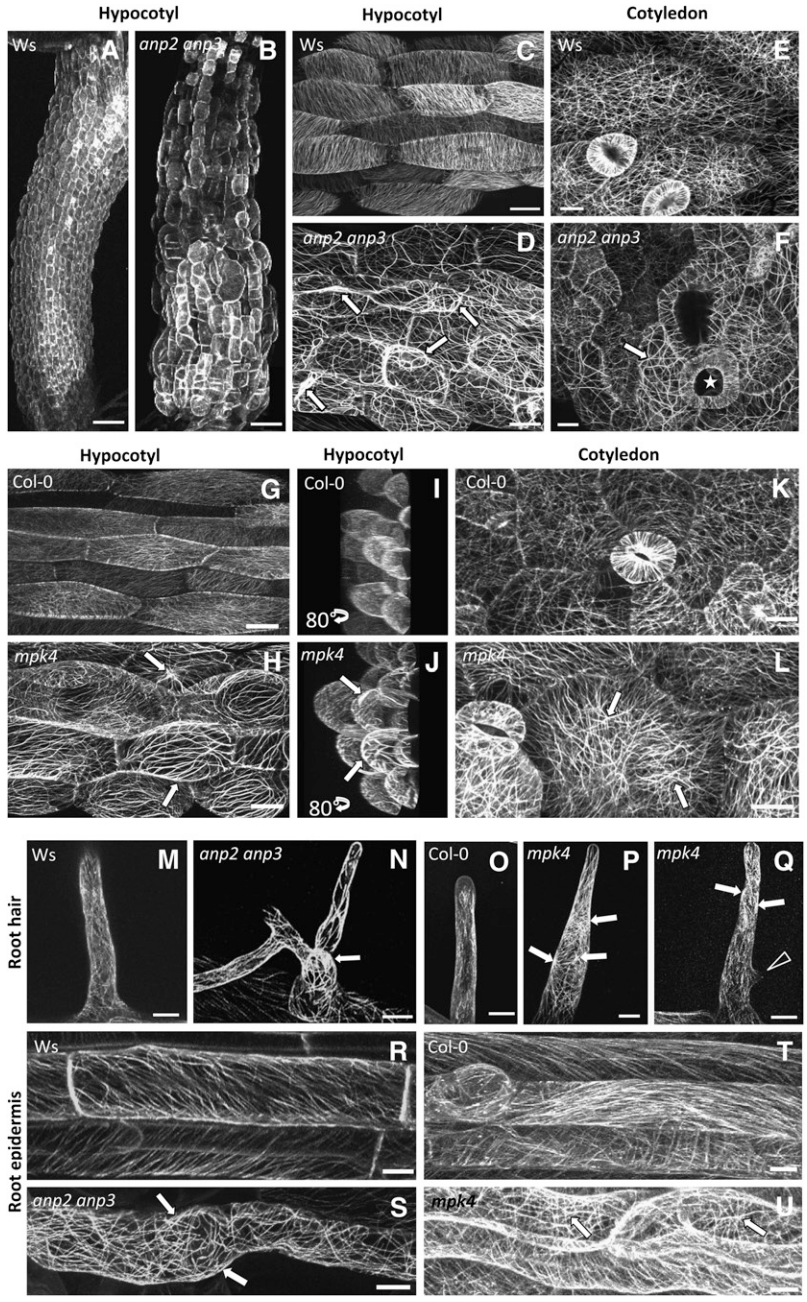

Figure 3. In Vivo Localization of MTs in Hypocotyls, Cotyledons, and Roots Using the *35S:GFP:MBD* Reporter Construct in *anp2 anp3* and *mpk4* Mutants.

(A) to **(F)** In vivo visualization of cortical MT organization using the *35S:GFP:MBD* construct and confocal laser scanning microscopy (CLSM) imaging in the hypocotyl and cotyledon of control (Ws) and *anp2 anp3* mutant plants. Disturbed patterns of cortical MT organization in hypocotyl and cotyledon cells of the *anp2 anp3* mutant as visualized in vivo using the *35S:GFP:MBD* construct. Note the extensive MT bundling as well as irregular and wavy configuration of the MT bundles (**[D]** and **[F]**, arrows). Irregularly formed and swollen cells are apparent in the hypocotyl (**[B]** and **[D]**) and cotyledon (**[F]**, star). Bars = 20 μm.

(G) to **(L)** In vivo visualization of cortical MT organization using the *35S:GFP:MBD* construct and CLSM imaging in the hypocotyl and cotyledon of control (Col-0) and *mpk4* mutant plants. Bundling of MTs in the cortex of hypocotyl and cotyledon cells (**[H]**, **[J]**, and **[L]**) in *mpk4* plants. Projection of hypocotyl cells, rotated by an angle of 80° to provide a lateral view (**[I]** and **[J]**). The cell volume of *mpk4* plants is significantly larger than that of Col-0. Arrows point to thick cortical MT bundles. Projection of 52 optical sections at a 0.65-μm step size **(I)**; z = 33.8 μm. Projection of 96 optical sections at a 0.65-μm step size **(J)**; z = 62 μm Bars = 20 μm.

(M) to **(Q)** In vivo visualization of MT organization using the *35S:GFP:MBD* construct and CLSM imaging in root hairs of control (Ws and Col-0) and

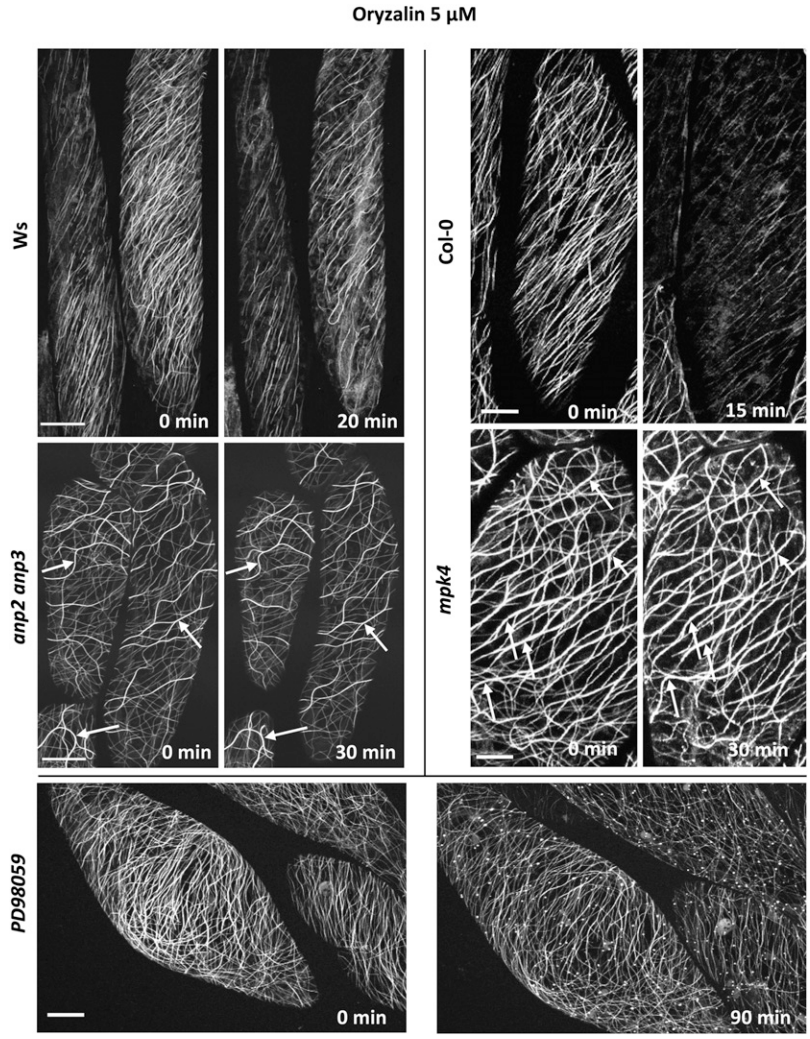

Figure 4. The Time-Dependent Response of Hypocotyl Epidermal Cells of *35S:GFP:MBD*-Transformed Ws/Col-0 and *anp2 anp3*/*mpk4* Plants Treated with 5 μM Oryzalin or with 20 μM PD98059 and 5 μM Oryzalin.

Note the severe depletion of cortical MTs in oryzalin-treated Ws and Col-0 hypocotyl epidermal cells after 20 min. By contrast, both individual MTs and/or MT bundles (arrows) persist in *anp2 anp3* and *mpk4* hypocotyl epidermal cells at least over a period of 30 min. In cells treated for 6 h with the MAPKK inhibitor PD98059 and subsequently with oryzalin plus PD98059, cortical MTs appear heavily bundled and randomly dispersed in the cell cortex, while remaining resistant to oryzalin treatment for at least 90 min. Time (in minutes) is indicated in the bottom right corner. Bars = 10 μm.

membrane (Figure 7A). This was in sharp contrast with the situation in the *anp2 anp3* cells, where MTs were extensively bundled. This mode of MT organization was not only observed in the cell cortex (Figure 7B), but also in transvacuolar cytoplasmic strands (Figure 7C) of all cell types examined. In some instances, large clusters of MTs were packed together with very little to virtually no space between individual MTs. Cross-linked MTs were spaced at distances ranging from 10 to 25 nm, while often electron-dense cross-bridges demonstrated a kinked, probably bipartite, structure (Figures 7B and 7C, arrows), consistent with

Figure 3. (continued).

mutant (*anp2 anp3* and *mpk4*) plants. Mutant root hairs with abnormal morphology, branched (**[N]** and **[Q]**, arrowhead), or swollen root hair bases **(P)** showing MT bundles (arrows) or disturbed MT orientation compared with wild-type root hairs (**[M]** and **[O]**). Bars = 10 μm.

(R) to **(U)** In vivo visualization of cortical MT organization using the *35S:GFP:MBD* construct and CLSM imaging in root epidermal cells of control (Ws and Col-0) and mutant (*anp2 anp3* and *mpk4*) plants. Patterns of cortical MT organization were disturbed in both mutants (**[S]** and **[U]**, arrows). Bars = 20 μm.

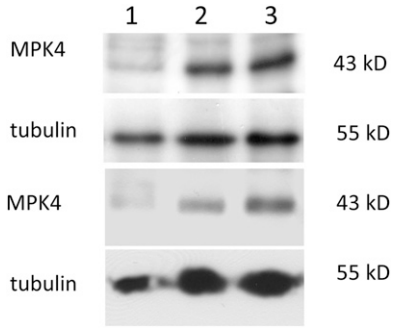

Figure 5. Association of MPK4 with the MT Surface.

Analysis of MT pellets from *Arabidopsis* extracts supplemented with exogenous bovine brain MTs (10 μM tubulin). Lane 1 shows the occurrence of MPK4 in the original supernatant (see Methods). Lanes 2 and 3 show the occurrence of MPK4 in the final MT pellets following the last glycerol cushion precipitation. In lane 3, the reaction mixture was supplemented with 10 μM 6×His-tagged MAP65-1. No significant difference can be detected in the efficiency of MPK4 coprecipitation in the presence or absence of MAP65-1. The bottom two rows show the same experiment in the absence of the glycerol cushion, which greatly enriches the amount of tubulin (bottom panel).

the idea that extensive MT bundling is due to the quantitative and functional upregulation of an MT-cross-linking MAP. Since a major MAP of this category is MAP65-1, which forms dimeric MT cross-bridges, we subsequently analyzed both *anp2 anp3* and *mpk4* mutants and the wild types for quantitative and qualitative changes of this MT-associated protein.

MAP65-1 and Bundled MTs in *anp2 anp3* and *mpk4* Mutants

ANP2 and ANP3, in analogy to the tobacco homolog NPK1, are expected to target MAP65-1 (Sasabe et al., 2006; Menges et al., 2008). Additionally, computer prediction analysis of phosphorylation sites has identified MAP65-1 as a putative MAPK target, and it has been confirmed experimentally that MAP65-1 is effectively phosphorylated by MPK4 and MPK6 (Smertenko et al., 2006). Therefore, we investigated the pattern of MAP65-1 localization in both the *anp2 anp3* and the *mpk4* mutants by double immunofluorescence labeling using specific MAP65-1 (Smertenko et al., 2004) and tubulin antibodies. In addition to published work (Smertenko et al., 2004), the specificity of the MAP65-1 antibody is shown here by immunoblotting. The antibody recognized a single band at 65 kD on the immunoblot prepared from *Arabidopsis* crude protein extract (see Supplemental Figure 7B online). As expected, in control root cells of Ws and Col-0 wild types (Figure 8), MAP65-1 localized discontinuously along the MT surface, showing more prominent staining in cortical sites with more prominent MT bundles (Figures 8A to 8C and 8J to 8L). The pattern of MAP65-1 distribution was remarkably different in the root cells of mutants when compared with respective controls in that the cortical MT system was strongly and evenly labeled along the entire length of the MTs, especially in the case of the thick cortical MT bundles (Figures 8D to 8I and 8M to 8R). Such decoration of entire cortical MTs with MAP65-1 was stronger in the *mpk4* mutant than in the *anp2 anp3* mutant (cf. Figures 8P to 8R with 8G to 8I). Negative controls, using the secondary antibodies alone, showed no fluorescence staining (see Supplemental Figure 8 online).

Altered Expression of MAP65 Isoforms in *anp2 anp3* and *mpk4* Mutants

The data derived from microscopy analysis further suggested the upregulation of MAP65-1 abundance in both the *anp2 anp3* and the *mpk4* mutants. However, more than one MAP65 isoform can be regulated by MAPK signaling. For this reason, we initially surveyed the MAP65 isoform complement by immunoblotting using an antibody raised against the CEEESWLEDYNR peptide of MAP65-1, which is conserved among all nine members of the MAP65 family (Mao et al., 2006). Probing Ws and Col-0 extracts with this antibody showed a most prominent signal at ~80 kD, probably corresponding to MAP65-3 and a weaker signal at 65

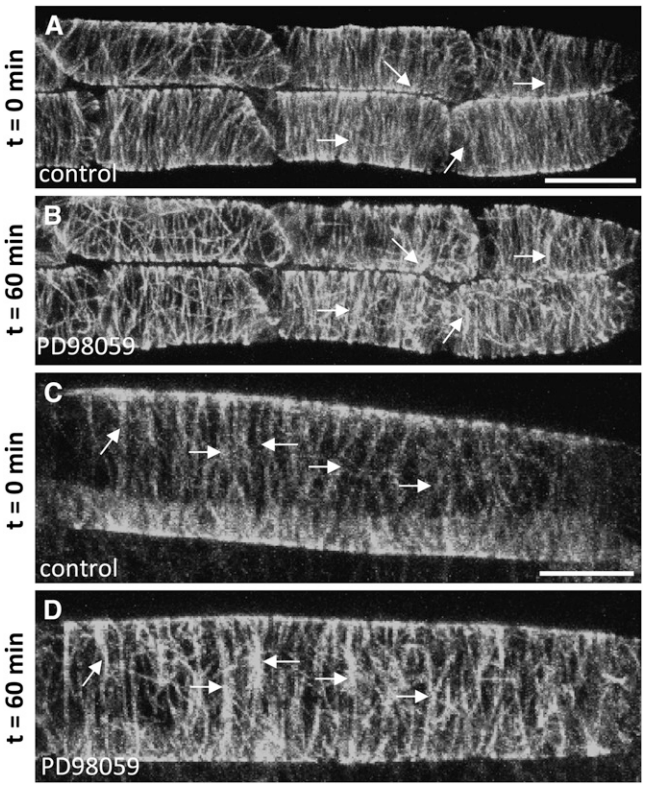

Figure 6. Effects of MAPKK Inhibitor PD98059 on Cortical MT Organization.

In vivo visualization of MTs in root epidermal cells of Col-0 plants stably transformed with *35S:GFP:MBD* construct. Arrows show examples of cortical MTs, which are aggregated into bundles at the end of the PD98059 treatment. Bars = 10 μm.

(A) and **(C)** Untreated control epidermal cells showing fine MTs of parallel orientation.

(B) and **(D)** The same cells as in **(A)** and **(C)** showing bundled and accumulated MTs in the cell cortex after 60 min treatment with PD98059 (20 μM).

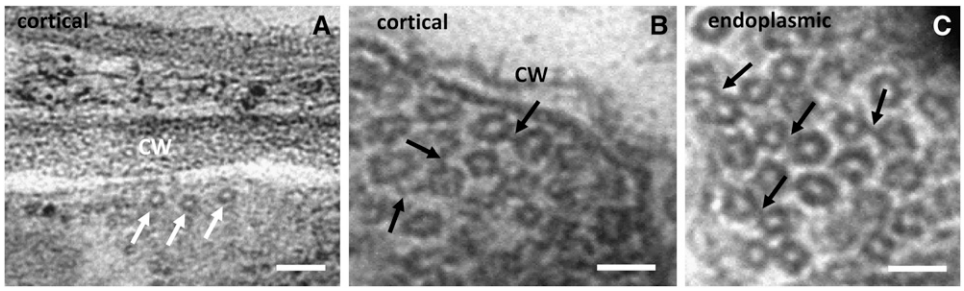

Figure 7. TEM Visualization of MT Organization in the Cortical Cytoplasm of Ws and the Cell Cortex or the Endoplasm of *anp2 anp3* Hypocotyl Epidermal Cells.

MTs are regularly spaced and loosely arranged in the vicinity of the plasma membrane in wild-type cells (**[A]**, arrows). MTs are densely packed and/or cross-linked in the cortical cytoplasm or the endoplasm in *anp2 anp3* cells (**[B]** and **[C]**). Black arrows denote cross-bridged MTs. CW, cell wall. Bars = 100 nm in **(A)** and 50 nm in **(B)** and **(C)**.

kD, probably corresponding to MAP65-1 (Hussey et al., 2002; Smertenko et al., 2008). Upon testing extracts of *anp2 anp3* and *mpk4*, we found a different pattern of MAP65 immunodetection compared with Ws and Col-0. In the cases of two mutants, the 80-kD band was diminished, while the 65-kD band was greatly upregulated (Figure 9A).

To document the identity of the bands that showed such differences, extracts were then analyzed with specific anti-MAP65-1 (Smertenko et al., 2004) and anti-MAP65-3 antibodies (Smertenko et al., 2008), which confirmed the upregulation of MAP65-1 and downregulation of MAP65-3 in both mutants compared with the corresponding wild types (Figure 9B). In addition to published work (Smertenko et al., 2004, 2008), the specificity of the anti-MAP65-1 and -MAP65-3 antibodies, which both recognize single bands of the expected molecular weight on immunoblots prepared from *Arabidopsis* crude protein extracts, is shown in Supplemental Figure 7B online. By analyzing MAP65-1 and MAP65-3 transcript levels by RT-PCR, we were not able to detect significant differences between the mutants and their corresponding wild types (Figure 9C), suggesting that the changes at the protein level were likely posttranscriptional. The above data are consistent with a role of MAP65-1 in the extensive bundling of cortical MTs.

Mode of MAP65 Isoform Regulation in *anp2 anp3* and *mpk4* Mutants

As MAP65-1 is a potential target for MAPK phosphorylation, we examined the phosphorylation status of this MAP in mutant versus wild-type plants to gain further insight into how the respective *anp2 anp3* and *mpk4* knockouts (Krysan et al., 2002; Nakagami et al., 2006) affect MT organization. For this purpose, we used a phosphoaffinity-based SDS-PAGE approach (Phos-Tag; Kinoshita et al., 2006) to analyze the phosphorylation status of MAP65-1 in protein extracts isolated from *anp2 anp3*, *mpk4*, Ws, and Col-0. Phos-Tag analysis and subsequent immunoblotting using the specific MAP65-1 antibody showed that the ratio of the phosphorylated form to the non-phosphorylated form of MAP65-1 is significantly decreased in the extracts of the *anp2 anp3* and *mpk4* mutants compared with the respective wild types (Figure 10A).

The specificity of the technique was confirmed by treating extracts with λ-phosphatase, which can effectively cleave phosphate groups from both Ser/Thr and Tyr residues (Figure 10B). Since, in unstressed plants, the activity of MPK4 is low (Nakagami et al., 2006), and because MAP65-1 is possibly a target of other kinases as well, we wanted to further substantiate the probability that the upper band in the Phos-Tag immunoblots is indeed related to MPK4-mediated phosphorylation. For this purpose, we boosted MPK4 activity by treating seedlings with 500 mM sorbitol to induce hyperosmotic stress (Ichimura et al., 2000), as shown in Supplemental Figure 7A online. In this case, we observed that the intensity of the upper phosphorylated MAP65-1 band was significantly enhanced (Figure 10B). When the same experiment was performed in the presence of the specific MAPKK inhibitor PD98059, the upper MAP65-1 band was diminished to nearly control levels (Figure 10B). Together, the results presented in Figure 10 and Supplemental Figure 7A online suggest that the upper band corresponds to the MAP65-1 pool that has been phosphorylated by MPK4.

It should be noted here that combined propidium iodide/fluorescein diacetate staining of Col-0 roots treated with 500 mM sorbitol (method described in Komis et al., 2006) revealed that root cells remain viable over a period exceeding 2 h (see Supplemental Figure 7 online).

Probing the Association of MAP65-1 with MPK4

The putative association between MAP65-1 and MPK4 was probed in cell extracts loaded with a 6×His-tagged fusion of recombinant native MAP65-1 and by coimmunoprecipitation analysis. Coimmunoprecipitation analysis was conducted using the MAP65-1 antibody and immunoblot detection of MPK4. In this case, MPK4 was detectable in the immunoprecipitate (Figure 11A). When 6×His-tagged MAP65-1 was pulled down by magnetic Ni-NTA agarose beads, MPK4 was prominently detected in the pellet, an observation compatible with previously published data (Smertenko et al., 2006) (Figure 11B). It must be noted that empty beads failed to retrieve MPK4 in the pellet, suggesting that the precipitation of MPK4 in the presence of 6×His-tagged MAP65-1 is rather specific.

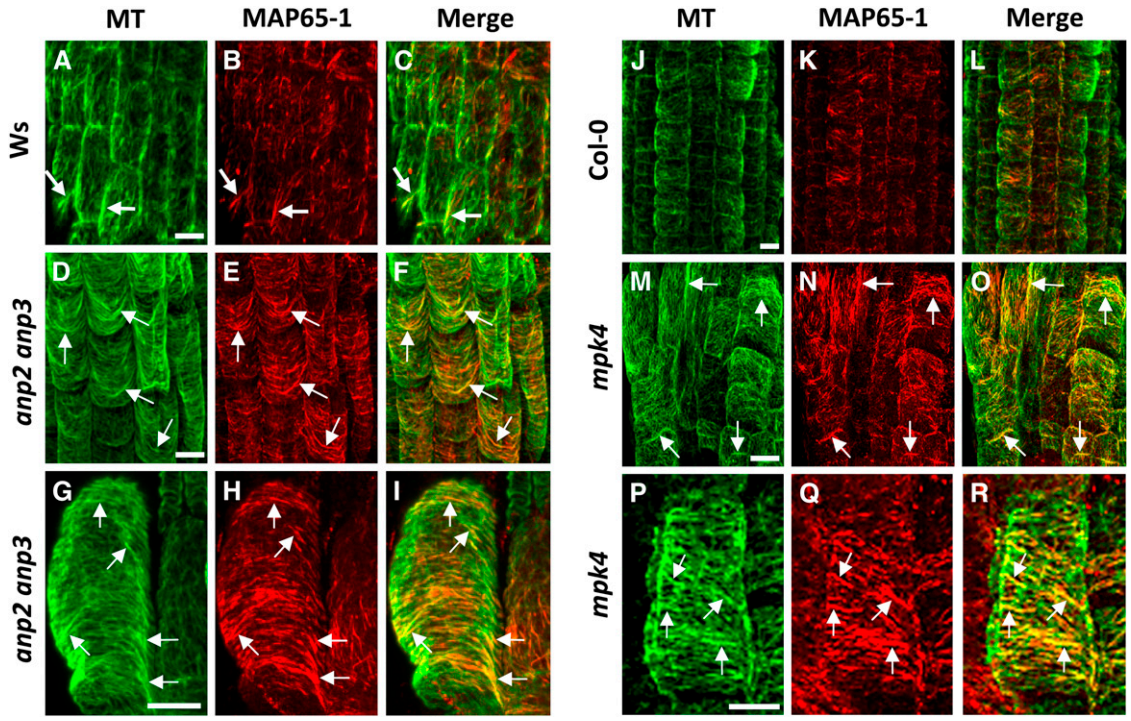

Figure 8. Patterns of MAP65-1 and Tubulin Immunofluorescence Localization in Roots of Control and Mutant Plants.

(A) to **(C)** Localization of MTs (green), MAP65-1 (red), and merged images in root epidermal cells of Ws. Note the partial spot-like colocalization of MAP65-1 with cortical MTs and the more extensive MAP65-1 decoration of certain MT bundles (arrows).
(D) to **(F)** The colocalization of MAP65-1 with bundled MTs (note increased yellow color in merged images) in root epidermal cells of *anp2 anp3* is much more extensive than in Ws (cf. Figure 9C), an observation consistent with the extensive cortical MT bundling found in this mutant. Arrows point to bundled MTs.
(G) to **(I)** Detailed visualization of the decoration of MTs by MAP65-1 in root epidermal cells of *anp2 anp3* showing extensive association of MAP65-1 with MT bundles (yellow color in merged image), often throughout their entire length.
(J) to **(L)** Overview of the localization of tubulin (green), MAP65-1 (red), and merged images in root epidermal cells of Col-0. Arrows point to bundled MTs.
(M) to **(O)** Overview of MAP65-1 distribution along cortical MTs in *mpk4* root epidermal cells. Note increased yellow color in merged image, suggesting extensive colocalization of MAP65-1 and bundled MTs in this mutant (arrows).
(P) to **(R)** Detailed view of MAP65-1 localization in *mpk4* root epidermal cells showing extensive association of MAP65-1 with MT bundles over their entire length (arrows).
Bars = 10 μm.

DISCUSSION

Molecular and Phenotypic Similarities between *anp2 anp3* and *mpk4* Mutants

In the literature, some molecular evidence has been presented supporting the case in favor of either interconnected or separate, though synergistic, functions of ANPs and MPK4. For example, both *anp2 anp3* and *mpk4* mutants display similar transcriptomic profiles and show upregulation of the pathogen response and resistance genes, such as PR1, chitinase, β-1,3-glucanase, and glutathione *S*-transferase (Petersen et al., 2000; Krysan et al., 2002). Moreover, NPK1 (an ANP homolog in tobacco) and MPK4 exert negative regulation on auxin signaling (Kovtun et al., 1998; Nakagami et al., 2006) and both ANP1 and MPK4 are involved in oxidative stress (Kovtun et al., 2000; Nakagami et al., 2006).

In this study, further evidence is provided to support a possible functional interplay between ANP2/ANP3 and MPK4. Thus, *anp2 anp3* and *mpk4* mutants show very similar phenotypes on the level of the whole organ as well as on the single cell level. All major vegetative organs of these mutants, such as roots, hypocotyls, cotyledons, and leaves, show disturbed growth patterns consistent with defective growth and morphogenesis, including bulging epidermal cells of the root and hypocotyl and leaf pavement cells with shallower indentations. Moreover, roots show radial expansion and root hairs of both mutants grow ectopically and develop abnormal, multiple branches. Further support comes from the cytological examination of the *mpk4* mutant, which exhibits cytokinetic defects that are consistent with the published cytokinetic phenotype of the *anp2 anp3* mutant (Krysan et al., 2002). Thus, the thorough phenotype, cytological, and molecular analyses reported here suggest that

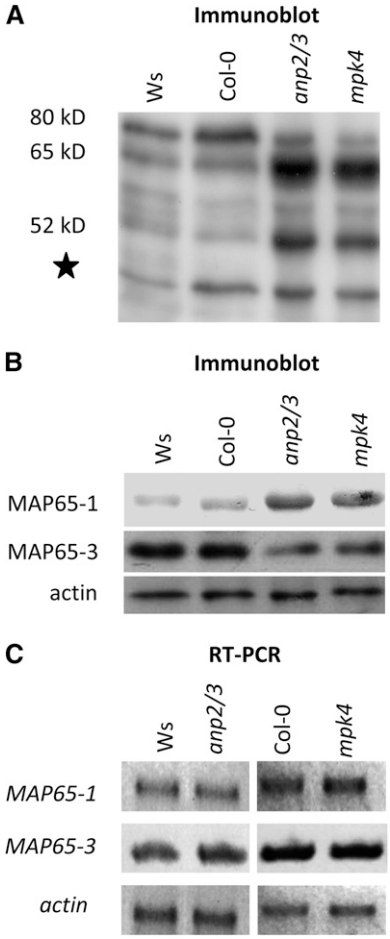

Figure 9. Comparative Analysis of MAP65 Isoform Composition and Expression Levels.

(A) and **(B)** General immunoblot survey of MAP65 isoform composition detectable with an anti-CEEESWLEDYNR antibody **(A)** or with isoform-specific anti-MAP65-1 and anti-MAP65-3 antibodies **(B)** showing quantitative upregulation of the MAP65-1 and downregulation of the MAP65-3 in both the *anp2 anp3* and the *mpk4* mutants compared with the respective Ws and Col-0 controls. Numbers indicate molecular mass in kilodaltons. The star denotes a band probably corresponding to a degradation product of MAP65. Anti-actin staining was used as a loading control **(B)**.

(C) RT-PCR analysis of *MAP65-1* and *MAP65-3* transcript levels (26 amplification cycles) showing no visible differences between Ws, *anp2 anp3*, Col-0, and *mpk4* plants. *ACTIN2* transcript (26 amplification cycles) was used as a loading control. Three biological and three technical replicates were performed.

ANP2, ANP3, and MPK4 likely function in a common developmental pathway that regulates the cellular morphogenesis, shape, and bundling of cortical MTs. At present, however, we cannot exclude the second possibility, namely, that ANP2/ANP3 and MPK4 function in independent synergistic pathways. Genetic studies are underway to clarify this point.

It is known that MPK4 can be activated through an upstream MAPKKK called MAP kinase or ERK kinase kinase 1 (MEKK1) during abiotic and biotic stress, but at the same time genetic and transcriptomic evidence suggests that this is not the only stress-activated MAPK pathway in *Arabidopsis* (Ichimura et al., 2006; Mészáros et al., 2006; Nakagami et al., 2006; Su et al., 2007; Suarez-Rodriguez et al., 2007). The *mekk1* and *mpk4* mutants exhibited a major physiological difference, whereas *mekk1* mutant growth is proportionally rescued by gradually increasing NaCl concentrations, growth of the *mpk4* mutant is completely inhibited by NaCl (Su et al., 2007). More importantly, from the developmental point of view, the *mekk1* and *mpk4* mutants show markedly different root and rosette leaf phenotypes (Nakagami et al., 2006; Su et al., 2007). While the *mekk1* mutant shows normal root outline and straight, albeit shorter, root hairs (Figure 2 in Nakagami et al., 2006), the *mpk4* mutant shows radial root

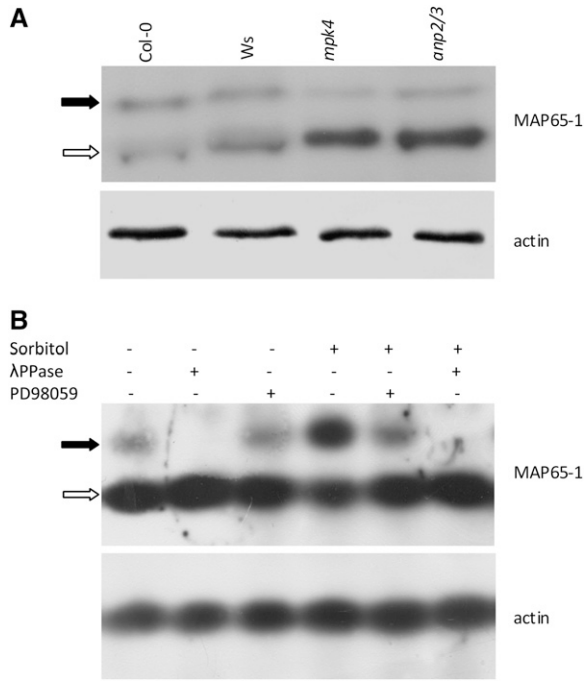

Figure 10. Analysis of the Phosphorylation Status of MAP65-1 Using Phos-Tag.

(A) Phos-Tag SDS-PAGE coupled to immunoblot detection using a MAP65-1–specific antibody. The black arrow indicates the phosphorylated form (top bands retarded in mobility), while the white arrow indicates the nonphosphorylated form (bottom bands). In both the *anp2 anp3* and the *mpk4* mutants, the relative amount of the phospho-MAP65-1 form was dramatically reduced compared with the total amount of the protein. Anti-actin staining was used as a loading control.

(B) Probing the efficiency of Phos-Tag technology to discriminate phosphorylated from nonphosphorylated MAP65-1 in Col-0 extracts subjected or not to hyperosmotic stress (500 mM sorbitol, 30 min) in the absence or presence of the MAPKK inhibitor PD98059 (20 μM, 2 h pretreatment followed by 30 min with 500 mM sorbitol). The bottom band (white arrow) represents the nonphosphorylated form of MAP65-1. The top band (black arrow) represents the phosphorylated form of MAP65-1, which diminished during the PD98059 treatment and was completely eliminated following λ-phosphatase (λPPase) treatment of the extract prior to electrophoresis.

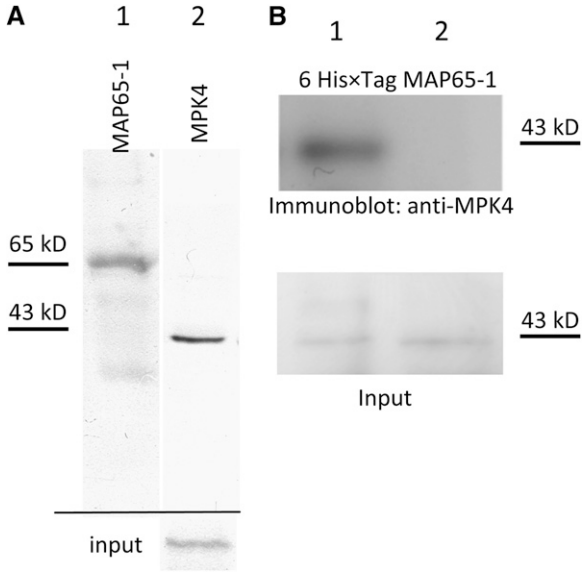

Figure 11. Putative Interactions between MPK4 and MAP65-1.

(A) Endogenous MAP65-1 was immunoprecipitated, and the final pellet was immunoblotted with anti-MAP65-1 (lane 1) or anti-MPK4 (lane 2). Input (bottom row) detects MPK4 in 10% of the original extract.
(B) Extracts (100 μg of total protein) were supplemented with 10 μM of recombinant 6×His-tagged MAP65-1 (lane 1) or with Ni-NTA agarose beads in the absence of 6×His-tagged MAP65-1 (lane 2). Input detects MPK4 in 10% of the original extract.

swelling and heavily branched root hairs, as shown in our study (Figures 1H and 1I). Thus, it is likely that MEKK1 is not integrated with MPK4 in the same pathway during plant development.

Phenotypes of *anp2 anp3* and *mpk4* Are Likely Related to MT Organization Defects

While defects in the actin organization and/or dynamics mostly result in changes in the root hair growth rate (Ketelaar et al., 2007) or in tip swelling (Ketelaar et al., 2007; Yang et al., 2007), pharmacological or genetic disturbances of MTs (Bibikova et al., 1999; Bao et al., 2001) consistently induce multiple branching, which is also the case in the mutants studied here. Most strikingly, *anp2 anp3* and *mpk4* mutants show an overall root malformation, which includes branched root hairs and severe root swelling. Radial root expansion is routinely observed in other MT mutants (e.g., *microtubule organization 1*; Whittington et al., 2001) or following pharmacological MT disruption (Baskin et al., 1994; Sugimoto et al., 2003; Collings et al., 2006; Gardiner et al., 2008). However, radial root expansion can also be the secondary consequence of reduced uniaxial growth in dwarfed mutants and might not be directly associated with MT defects. An example of the above can be found in the *radially swollen 1*, *4*, and *7 Arabidopsis* mutants, showing lateral expansion of the root but normal, transverse cortical MT configuration (Sugimoto et al., 2001; Wiedemeier et al., 2002). Thus, the best diagnostic criterion for an MT deficiency in both *anp2 anp3* and *mpk4* mutants is the combination of radial root swelling with severely compromised root hair growth, which in most cases is multiaxial, resulting in the formation of branched root hairs.

Impaired MT Organization as a Consequence of Defective MAPK Signaling

When MT organization was studied in situ and in vivo in root and hypocotyls epidermal cells of both mutants, it showed randomly dispersed patterns considerably deviating from the parallel, transverse configurations of wild-type cells. Furthermore, MTs appear heavily bundled, most likely due to extensive cross-linking as shown by TEM. Although in many cases MTs appear tightly packed, TEM observations revealed kinked, bipartite, electron-dense cross-bridges. Additionally, MTs from both mutants showed profound resistance to moderate oryzalin treatments. The possibility that such defects are a consequence of impaired MAPK signaling was further addressed in wild-type root epidermal cells treated with the potent MAPKK inhibitor, PD98059. In this case, the inhibitor caused bundling of cortical MTs, similar to that observed in the mutants, but to a lesser extent.

Recruitment of MPK4 to MTs

Since the phenotypes observed in both mutants are most likely MT related, we postulated that at least a fraction of MAPKs in control plants would be physically associated with MTs.

Biochemical analysis demonstrated that MPK4 (Figure 5) and MPK6 (Müller et al., 2010) consistently coprecipitate with exogenous MTs in cell-free extracts of wild-type *Arabidopsis* seedlings. Previously, it was shown in many eukaryotes that MAPKs associate with MTs. This form of association is conditional or constitutive (Reszka et al., 1995, 1997, and references therein), although the mechanism of binding may require another factor because an MT binding domain in the MAPK peptide sequences has not yet been identified. In neuronal cells, c-Jun N-terminal MAPKs (JNKs) associate with the MT surface through their interaction with JIPs (JNK-interacting proteins), which in turn are coupled to conventional kinesins (Koushika, 2008). In human neutrophils, ERKs, although massively relocated to the nucleus upon induction, remain to a significant extent associated with the radial, perinuclear MT system (Reszka et al., 1995). Finally, the p38/SAPK1/Hog1 MAPK contributes to the regulation of MT dynamics by targeting the catastrophe-promoting protein stathmin/Op18 to the MTs (Parker et al., 1998).

In higher plants, the interplay between MT organization and MAPK signaling has been demonstrated in a few cases. Recently, Walia et al. (2009) showed that MPK18 and the MAPK phosphatase PHS1 (propyzamide hypersensitive 1) act in a complementary fashion to regulate MT organization and dynamics. Because the complex of PHS1 and MPK18 does not localize to MTs, its relationship to MT dynamics may require the targeting of a substrate that transiently binds to the MT surface in relation to its phosphorylation status. Individual components of the above complex were also not shown to interact directly with MTs; however, genetic evidence showed a potential interaction between PHS1 and MOR1 (a member of the XMAP-family),

linking the respective pathway to MT regulation (Naoi and Hashimoto, 2004).

The functional association between MAPKs and MTs is better understood during the mitotic and cytokinetic progression in higher plants. Examples of MAPKs previously shown to physically interact with and regulate mitotic/cytokinetic MT arrays include the MMK3 of alfalfa (Bögre et al., 1999, 2000) and the F6 and the NACK-PQR members of *N. tabacum* (Calderini et al., 1998; Takahashi et al., 2004); however, similar functions remain to be identified for the respective homologs of *Arabidopsis*.

Computer prediction and experimental studies in plants have already revealed potential MAPK targets as MT binding proteins. Putative ERK binding motifs have been identified so far in MOR1 and in MAP65-1 (Smertenko et al., 2006; Walia et al., 2009).

The MAP65 Family as a Primary and Secondary MAPK Signaling Target

The best-studied examples of MAPK-targeted MAPs are the members of the MAP65 family, MAP65-1, MAP65-2, and MAP65-3. Among them, MAP65-1 is robustly phosphorylated by both MPK4 and MPK6 (Smertenko et al., 2006), while MAP65-2 and MAP65-3 have been experimentally demonstrated to be phosphorylated by the heterologous protein in tobacco, NRK1 (Sasabe et al., 2006). It is interesting that, at least in the case of MAP65-1, the single MAPK targeting motif is situated at the C-terminal MT binding domain and overlaps with a CDK targeting site (Smertenko et al., 2006). This suggests that MAPK-mediated phosphorylation of MAP65-1 may interfere with its MT binding affinity, while also explaining the differential localization of MAP65-1 during mitotic progression, as a function of its phosphorylation status (Smertenko et al., 2004, 2006; Chang et al., 2005; Mao et al., 2006).

By comparing the expression of the MAP65 family complement of the *anp2 anp3* and the *mpk4* mutants with that of the Ws and Col-0 wild types, respectively, it became apparent that, although we could detect differences in the levels of the phosphorylated MAP65-1, there were also quantitative differences in the overall amount of some MAP65 isoforms, of which MAP65-1 and MAP65-3 were further studied. Briefly, the levels of MAP65-1 were upregulated in both mutants, whereas MAP65-3 levels were diminished in the mutants. These changes in protein level both seem to be posttranscriptional, as the amounts of corresponding transcripts remained roughly unchanged. Additionally, the depletion of MAP65-3 in both mutants is not sufficient to explain their MT features, since it is, similarly to MAP55-1, also an MT cross-linker (Müller et al., 2004). However, since localization of MAP65-3 is predominantly mitotic/cytokinetic (Müller et al., 2004; Caillaud et al., 2008; Smertenko et al., 2008), its contribution to the phenotypes and the interphase MT organization observed here should be negligible.

The excessive amounts of MAP65-1 alone can sufficiently explain the massive cortical MT bundling (Van Damme et al., 2004; Mao et al., 2006; Gaillard et al., 2008) and moderate drug stability (Van Damme et al., 2004; Wasteneys and Ambrose, 2009) seen in both mutants. The upregulated MAP65-1 levels seemed to coincide with the increased occurrence of MAP65-1 along MT bundles and the extended degree of MT cross-linking in root whole-mount immunofluorescence samples of *anp2 anp3* and *mpk4*, as opposed to the patchy pattern of MAP65-1 distribution and the sparser cortical MT arrangement commonly observed in root whole mounts of the wild types.

If MAP65-1 associates with and is regulated by MPK4, then these two proteins would have to physically interact. This possibility was explored by coimmunoprecipitation assays. Specific MAP65-1 antibodies pulled down MPK4, and recombinant 6× His-tagged MAP65-1 copelleted with MPK4. The above results are in accordance with previously published data (Smertenko et al., 2006). Due to the nature of these assays, it cannot be determined if MAP65-1 and MPK4 interact when one or both partners are bound to the MT surface or when they are dissociated from it.

In addition to the above, MAP65-1 is underphosphorylated in extracts of both *anp2 anp3* and *mpk4* mutants. Diminished amounts of phosphorylated MAP65-1 can further add to the extent of MT cross-linking by diminishing its affinity toward the MT surface, since the phosphorylation status of MAP65-1 is directly proportional to its MT binding capacity. An engineered form of MAP65-1 with multiple phosphomimetic substitutions encompassing every putative phosphorylation site on its primary structure results in a dramatic reduction of its MT binding capacity as assessed in MT coprecipitation assays, without affecting MT dynamics (Smertenko et al., 2006). The amounts of multiphosphomimetic MAP65-1 coprecipitating with MTs are much lower than those of the native protein or of a phosphomimetic analog excluding the MAPK site (Smertenko et al., 2006). This prompts us to suggest that MAP65-1 underphosphorylation in the MAPK mutants is a significant contributor to MT bundling and disorientation, in addition to the upregulation of MAP65-1 overall levels.

In conclusion, this study reveals a previously unidentified role of a major stress-activated *Arabidopsis* MAPK, namely MPK4, in plant development; MPK4 regulates the spatial and temporal aspects of cortical MT organization. MAP65-1 is indicated as a putative target of MPK4; however, further molecules that interact with MPK4 may regulate MT organization and dynamics.

METHODS

Plant Materials and Phenotype Analysis

Col-0 and Ws ecotypes of *Arabidopsis thaliana* were used throughout. Double homozygous negative mutants of the MAPKKK genes *ANP*2 and *ANP*3 were isolated through screens of T-DNA insertional mutants by Krysan et al. (2002) raised in a Ws background. Homozygous mutants of the *MPK4* gene (*mpk4*) in a Col-0 background were selected from seeds of heterozygous plants on the basis of phenotype and kanamycin resistance (Nakagami et al., 2006). For phenotyping, mutant and wild-type seeds were germinated on Phytagel-solidified, sucrose supplemented half-strength Murashige and Skoog medium at pH 5.8 without vitamins and allowed to grow for 4 to 12 d. Prior to germination, seeds were surface sterilized with commercial bleach supplemented with 0.1% (v/v) Triton X-100 and thoroughly rinsed with sterile, distilled water. Plants were also germinated and grown in soil for 4 to 6 weeks to observe rosette leaf phenotypes. Plants were grown in a controlled temperature and photoperiod chamber at 22°C and a 16 h/8 h light/dark cycle.

Seedlings of *anp2 anp3* and *mpk4* mutants were then observed and documented with a Leica MZ FLIII stereomicroscope coupled to a JVC

CCD camera KY-F70B running under the Diskus software (Carl Hilgers). Seedlings were screened for root and hypocotyl aberrations involving gross structure of the above tissues and subsequently the morphology of root and hypocotyl epidermal cells and root hairs. Morphometric aspects of discrete phenotypes included root length and width as well as root hair morphology.

For more detailed analysis of the root phenotype, mutant and wild-type seedlings were fixed and embedded in Spur's resin (see below), and semithin cross sections of the roots were produced. The cross sections were stained with 1% (w/v) tolouidine blue in 1% (w/v) aqueous borax and documented under the microscope (Leica DM 5500B) as previously described (Komis et al., 2002).

Antibodies and Reagents

All chemicals were of analytical grade and purchased from Sigma-Aldrich, Roth, and Serva, unless stated otherwise. For immunofluorescent localizations and for immunoblot analysis, the following primary and secondary antibodies were used: rabbit polyclonal anti-CEEESWLEDYNR (kindly provided by Clive W. Lloyd, John Innes Center, UK), rabbit polyclonal anti-MAP65-1 and mouse polyclonal anti MAP65-3 (kindly provided by Andrei Smertenko, University of Durham, UK), and rabbit polyclonal anti-MPK4 (Sigma-Aldrich). For root whole-mount immunofluorescence, fluorescein isothiocyanate- or tetramethyl rhodamine isothiocyanate-coupled anti-mouse and anti-rabbit IgGs (Sigma-Aldrich) were used as secondary antibodies. Primary antibodies were detected on immunoblots by alkaline phosphatase or horseradish peroxidase–conjugated anti-rabbit or anti-mouse IgGs (Promega and Cell Signaling, respectively).

Generation of Promoter GUS Constructs and Transgenic *Arabidopsis* Lines

The 2-kb putative promoter upstream region encoding MPK4 was amplified from genomic DNA of *Arabidopsis* Col-0 with the following primer pair: 5′-GCGGATCCGAAGAAGAACAATGCTCG-3′ and 5′-GCCCCGGGCGGAGCAAAATTCCTCAC-3′. Additionally, *Bam*HI and *Sma*I restriction sites were inserted, and the promoter sequence was cloned into the ΔGUS vector (Topping et al., 1994). The clones were verified by sequencing and the DNA was used for the transformation of *Agrobacterium tumefaciens* strain GV3101. Transgenic plants were generated by the floral dipping method (Clough and Bent, 1998).

GUS Staining Procedure

Transgenic T1 and T2 plants carrying the *ProMPK4:GUS* construct were selected on phytagel sucrose medium supplemented with 25 μg/mL of kanamycin. Kan-resistant seedlings were selected for staining. All samples were processed according to De Block and Debrouwer (1992) with 1 mM 5-bromo-4-chloro-3-indolyl-D-glucuronide in staining buffer (0.1 M sodium phosphate, pH 7.0, 0.01 M EDTA, 0.5 mM $FeK_3[CN]_6$, and 0.1% [v/v] Triton X-100) at 37°C for 2 to 18 h. Specimens were cleared with 1:1 ethanol/acetic acid, examined, and documented under the stereomicroscope as described above.

Whole-Mount Immunofluorescence Labeling

Whole seedlings of wild types and mutants were prepared for immunofluorescent localizations according to standard procedures (Sauer et al., 2006; Müller et al., 2010) and probed with the appropriate antibodies. Stained samples were observed and documented with an Olympus FV1000 CLSM system. Fluorescein isothiocyanate fluorescence was imaged using excitation with the 488-nm line of a multiline argon laser and a 500- to 535-nm band-pass emission filter. Tetramethyl rhodamine isothiocyanate fluorescence was excited by the 543-nm laser line and detected with a 560- to 660-nm emission filter. TIFF images of Z-stacks were converted to maximum intensity projections using Olympus FV10-ASW 1.7 software.

TEM

For TEM and semithin sectioning, whole-mutant or wild-type seedlings were fixed, embedded in Spur's resin, sectioned, and contrasted as previously described (Komis et al., 2002), with the exception that samples were mordanted with 4% (w/v) tannic acid in 100 mM phosphate buffer, pH 7.8, following glutaraldehyde fixation and with 8% (w/v) tannic acid following OsO_4 postfixation to facilitate MT visualization. TEM samples were observed and documented using a Leo 920AB TEM (Zeiss).

RNA Extraction and RT-PCR

Total RNA was isolated from *Arabidopsis* seedlings with the TRI reagent according to the manufacturer's instructions (Molecular Research Center). RT-PCR was performed using the SuperScript III One-Step RT-PCR system with Platinum Taq DNA polymerase (Invitrogen). Approximately 0.1 μg of total RNA was used for each RT-PCR analysis. Amplified transcripts included *MPK4*, *MAP65-1*, and *MAP65-3*. For each analysis, the following pairs of primers were used: *MPK4* forward, 5′-GCGGATCCATGTCGGCGGAGAGTTGTTTC-3′, reverse, 5′-GCACTAGTTCACACTGAGTCTTGAGG-3′; *MAP65-1*: forward, 5′-ATGGCAGTTACAGATACTGAA-3′, reverse, 5′-TCATGGTGAAGCTGGAACT-3′; *MAP65-3*: forward, 5′-ATGGCAAGTGTTCAAAAA-3′, reverse, 5′-TCAAACCAAACGACATTC-3′; *ACTIN2*: forward, 5′-GCGGATCCATGGCTGAGGCTGATGATATTCAACC-3′, reverse, 5′-CGTTAGACCATGGAACATTTTCTGTGAACGATTCC-3′. Conditions of RT-PCR included the following: for *MPK4* amplification, annealing at 55°C for 30 s and elongation at 72°C for 1 min. Cycles varied from 25 to 30. For *MAP65-1* amplification, annealing was at 60°C for 30 s and elongation at 72°C for 1 min. Cycles varied from 25 to 30. For *MAP65-3* amplification, annealing was at 50°C for 30 s and elongation at 72°C for 2 min. Cycles varied from 25 to 30. Products were visualized by ethidium bromide.

Coprecipitation of Interacting Proteins with Recombinant MAP65-1

Bacteria expressing 6×His-tagged MAP65-1 (Smertenko et al., 2006) were inoculated in liquid Luria-Bertani medium supplemented with kanamycin (100 μg/mL) and cultured overnight to an OD_{600} of 0.2 to 0.4. Subsequently, protein expression was induced with 1 to 10 mM of isopropyl β-D-1-thiogalactopyranoside for 2 to 4 h. Finally, cultures were briefly pelleted at 3000 rpm for 5 min, and pellets were rapidly resuspended in ice-cold extraction buffer and tip sonicated at 4 × 10 s bursts on ice (maximum power). Following clearing (20,000*g*, 2°C, 10 min), the protein extract was bound on Ni-NTA spin columns (Qiagen) according to the manufacturer's instructions and eluted with increasing imidazole concentrations in extraction buffer (A. Smertenko, personal communication). The final eluates were diafiltrated and concentrated to 1 mg of protein/mL (Microcon YM10, 10 kD cutoff; Millipore) with MSB supplemented with 50% (v/v) of glycerol and either flash frozen in liquid nitrogen (LN_2) and stored at –80°C until later use or used directly for MT binding assays or copelleting assays with *Arabidopsis* protein extracts. For the latter, purified 6×His-tagged proteins were bound on BSA-treated Ni-NTA magnetic agarose beads (Qiagen) and added to a total of 5 μM recombinant protein per 100 μg of total protein. The beads were magnetically recovered (Ni NTA magnetic agarose beads and 12-tube magnet both from Qiagen), washed thoroughly with MSB buffer, and finally resuspended in Laemmli sample buffer. Following heat denaturation, proteins were resolved by 10% SDS-PAGE and analyzed by immunoblot analysis for suspected coprecipitating species.

Coprecipitation of Proteins with in Vitro–Assembled MTs

MT-interacting species were retrieved from high-speed supernates (40,000*g*, 20°C, 30 min) of *Arabidopsis* seedlings homogenized on ice with 2 volumes of BRB80 buffer (80 mM K-PIPES, pH 6.8, 5 mM EGTA, and 5 mM $MgSO_4 \times 7H_2O$) supplemented with 1 mM GTP, 5 μM oryzalin, and one tablet of the EDTA-free Complete protease inhibitor cocktail (Roche). The cleared cytosolic extract was exogenously fed with 10 μM bovine brain MTs prepared in BRB80 buffer (Cytoskeleton), 10 μM taxol, and 1 mM GTP. In some cases, 10 μM purified 6×His-tagged MAP65-1 was also added to the reaction. Following a 30-min incubation at room temperature, MTs and interacting proteins were precipitated three times over a 20% glycerol cushion prepared in BRB80 buffer supplemented with 1 mM GTP and 10 μM taxol. Alternatively, precipitations were performed without a glycerol cushion. This improved the yield of precipitated proteins but probably partially compromised the specificity of the assay. The final pellet was resuspended in Laemmli sample buffer, boiled, and directly used for SDS-PAGE/immunoblot analysis.

Coimmunoprecipitations

For coimmunoprecipitation analysis, *Arabidopsis* extracts were prepared by homogenizing liquid nitrogen powders in G-buffer (Komis et al., 2004). Following protein content measurements, 1 to 2 mg of total protein was cleared with 50 μL of 50% (w/v) protein A-agarose beads slurry. Subsequently, samples were incubated with 2 to 5 μg of antibody and 50 μL of protein A-coupled agarose beads for 3 to 4 h at 40°C, washed four times with G-buffer, rinsed twice with immunoprecipitation buffer (20 mM Tris-HCl, pH 7.5, 150 mM NaCl, and 5 mM EGTA), and finally denatured with Laemmli sample buffer at 90°C. The protein pattern was resolved by SDS-PAGE and analyzed by immunoblot analysis (immunoprecipitation: MAP65-1 antibody, immunoblot MPK4 antibody). Input control contained 10% of the original extract used for coimmunoprecipitations.

Analysis of Phosphorylated Proteins

Acrylamide copolymerized-Phos-Tag chelates phosphorylated moieties in proteins in the presence of Mn^{2+}, thus inducing a mobility retardation of phosphorylated proteins on Phos-Tag/Mn^{2+}-copolymerized SDS-PAGE gels compared with their nonphosphorylated counterparts, which in turn results in the discrimination of the phospho- and the nonphosphorylated forms (Kinoshita et al., 2006). Thus, phosphorylated proteins appear as double or multiple bands following immunoblotting, depending on the phosphorylation degree. Phos-Tag technology has been used successfully in numerous cases for animal proteins (e.g., Kinoshita et al., 2006, 2009; Gallon, 2008; Oh and Irvine, 2008; Sikkema et al., 2009; Deswal et al., 2009) and also in plant protein phosphorylation studies (e.g., Bethke et al., 2009; Panteris et al., 2010). This assay was performed in extracts from mutant or wild-type *Arabidopsis* plants obtained from the homogenization of liquid nitrogen powders in G-buffer from which β-glycerophosphate was omitted because it would interfere with Phos-Tag mobility retardation (Kinoshita et al., 2006). This extract was used directly after protein quantitation by the Bradford assay. Proteins were resolved by 7.5 to 10% SDS-PAGE and analyzed by means of immunoblot analysis. To facilitate adequate separation between phospho- and nonphospho forms, the gel was run until the 25-kD prestained marker eluted from the gel. To verify that the additional bands observed after separation on Phos-Tag gels were due to phosphorylation, a portion of the original extract was treated with lambda phosphatase (New England Biolabs) according to the manufacturer's instructions and analyzed likewise. To test whether the additional Phos-Tag bands were eliminated due to λ-phosphatase action, an aliquot was treated with λ-phosphatase in the presence of phosphatase inhibitors, 10 mM NaF and 1 mM Na_3VO_4. As positive controls, protein extracts from plants conditioned by MAPK activating hyperosmotic stress were used, either in the absence or in the presence of 20 μM PD98059 MAPKK inhibitor.

Accession Numbers

Sequence data from this article can be found in the Arabidopsis Genome Initiative or GenBank/EMBL databases under the following accession numbers: At4g01370 (MPK4), At1g54960 (ANP2), and At3g06030 (ANP3).

Supplemental Data

The following material is available in the online version of this article.

Supplemental Figure 1. Phenotypic Comparison of the Rosette Leaves of 4-Week-Old *mpk4* and Col-0 Plants.

Supplemental Figure 2. Root Growth of *anp2 anp3* and *mpk4* Seedlings.

Supplemental Figure 3. Ectopic Root Hairs in *anp2 anp3* and *mpk4* Mutants.

Supplemental Figure 4. Radial Swelling of Root Cells in the *mpk4* Mutant.

Supplemental Figure 5. Analysis of Tissue- and Cell-Specific Expression of *MPK4*.

Supplemental Figure 6. Effect of PD98059 on MPK4 Activation and Specificity of MPK4, MAP65-1, and MAP65-3 Antibodies.

Supplemental Figure 7. Cell Viability Assessment in *Arabidopsis* Roots Using Dual Propidium Iodide/Fluorescein Diacetate Staining.

Supplemental Figure 8. Negative Controls for Immunofluorescent MAP65-1 and Tubulin Staining.

ACKNOWLEDGMENTS

This work was supported by Deutsche Forschungsgemeinshaft Grants Nr. SA 1564/1-2 and SA 1564/2-3, a postgraduate fellowship from the University of Bonn to M.B, and an Alexander von Humboldt postdoctoral fellowship to G.K. We acknowledge expert technical assistance by Claudia Heym and Ulla Mettbach and helpful comments by both anonymous reviewers and by members of the Bonn laboratory. We thank Patrick Krysan, Heribert Hirt, Clive Lloyd, and Andrei Smertenko for providing material and advice.

Received September 29, 2009; revised February 8, 2010; accepted February 27, 2010; published March 9, 2010.

REFERENCES

Akhmanova, A., and Steinmetz, M.O. (2008). Tracking the ends: A dynamic protein network controls the fate of microtubule tips. Nat. Rev. Mol. Cell Biol. **9:** 309–322.

Bao, Y., Kost, B., and Chua, N.H. (2001). Reduced expression of alpha-tubulin genes in *Arabidopsis thaliana* specifically affects root growth and morphology, root hair development and root gravitropism. Plant J. **28:** 145–157.

Baskin, T.I., Wilson, J.E., Cork, A., and Williamson, R.E. (1994). Morphology and microtubule organization in Arabidopsis roots exposed to oryzalin or taxol. Plant Cell Physiol. **35:** 935–942.

Bethke, G., Unthan, T., Uhrig, J.F., Pöschl, Y., Gust, A.A., Scheel, D., and Lee, J. (2009). Flg22 regulates the release of an ethylene

response factor substrate from MAP kinase 6 in *Arabidopsis thaliana* via ethylene signaling. Proc. Natl. Acad. Sci. USA **106:** 8067–8072.

Bibikova, T.N., Blancaflor, E.B., and Gilroy, S. (1999). Microtubules regulate tip growth and orientation in root hairs of *Arabidopsis thaliana.* Plant J. **17:** 657–665.

Bögre, L., Calderini, O., Binarova, P., Mattauch, M., Till, S., Kiegerl, S., Jonak, C., Pollaschek, C., Barker, P., Huskisson, N.S., Hirt, H., and Heberle-Bors, E. (1999). A MAP kinase is activated late in plant mitosis and becomes localized to the plane of cell division. Plant Cell **11:** 101–113 .

Bögre, L., Calderini, O., Merskiene, I., and Binarova, P. (2000). Regulation of cell division and the cytoskeleton by mitogen-activated protein kinases in higher plants. Results Probl. Cell Differ. **27:** 95–117.

Caillaud, M.C., Abad, P., and Favery, B. (2008). Cytoskeleton reorganization, a key process in root-knot nematode-induced giant cell ontogenesis. Plant Signal. Behav. **3:** 816–818.

Calderini, O., Bögre, L., Vicente, O., Binarova, P., Heberle-Bors, E., and Wilson, C. (1998). A cell cycle regulated MAP kinase with a possible role in cytokinesis in tobacco cells. J. Cell Sci. **111:** 3091–3100.

Cassimeris, L., and Spittle, C. (2001). Regulation of microtubule-associated proteins. Int. Rev. Cytol. **210:** 163–226.

Chang, H.Y., Smertenko, A.P., Igarashi, H., Dixon, D.P., and Hussey, P.J. (2005). Dynamic interaction of NtMAP65–1a with MTs in vivo. J. Cell Sci. **118:** 3195–3201.

Clough, S.J., and Bent, A.F. (1998). Floral dip: A simplified method for Agrobacterium-mediated transformation of *Arabidopsis thaliana.* Plant J. **16:** 735–743.

Collings, D.A., Lill, A.W., Himmelspach, R., and Wasteneys, G.O. (2006). Hypersensitivity to cytoskeletal antagonists demonstrates microtubule-microfilament cross-talk in the control of root elongation in *Arabidopsis thaliana.* New Phytol. **170:** 275–290.

De Block, M., and Debrouwer, D. (1992). *In situ* enzyme histochemistry on plastic-embedded plant material. The development of an artefact-free 3-glucuronidase assay. Plant J. **2:** 261–266.

Desai, A., and Mitchison, T.J. (1997). Microtubule polymerization dynamics. Annu. Rev. Cell Dev. Biol. **13:** 83–117.

Deswal S., Beck-García K., Blumenthal B., Dopfer E.P., and Schamel W.W. (2009). Detection of phosphorylated T and B cell antigen receptor species by Phos-tag SDS- and Blue Native-PAGE. Immunol. Lett., in press.

Gaillard, J., Neumann, E., Van Damme, D., Stoppin-Mellet, V., Ebel, C., Barbier, E., Geelen, D., and Vantard, M. (2008). Two microtubule-associated proteins of Arabidopsis MAP65s promote antiparallel microtubule bundling. Mol. Biol. Cell **19:** 4534–4544.

Gallon, C.E. (2008). Current techniques for the study of troponin I phosphorylation in human heart. J. Muscle Res. Cell Motil. **29:** 169–172.

Gardiner, J., Andreeva, Z., Barton, D., Ritchie, A., Overall, R., and Marc, J. (2008). The phospholipase A inhibitor, aristolochic acid, disrupts cortical microtubule arrays and root growth in Arabidopsis. Plant Biol. **10:** 725–731.

Granger, C.L., and Cyr, R.J. (2001). Spatiotemporal relationships between growth and microtubule orientation as revealed in living root cells of *Arabidopsis thaliana* transformed with green-fluorescent-protein gene construct GFP-MBD. Protoplasma **216:** 201–214.

Hussey, P.J., Hawkins, T.J., Igarashi, H., Kaloriti, D., and Smertenko, A. (2002). The plant cytoskeleton: Recent advances in the study of the plant MT-associated proteins MAP-65, MAP-190 and the Xenopus MAP215-like protein, MOR1. Plant Mol. Biol. **50:** 915–924.

Ichimura, K., Casais, C., Peck, S.C., Shinozaki, K., and Shirasu, K. (2006). MEKK1 is required for MPK4 activation and regulates tissue-specific and temperature-dependent cell death in Arabidopsis. J. Biol. Chem. **281:** 36969–36976.

Ichimura, K., Mizoguchi, T., Yoshida, R., Yuasa, T., and Shinozaki, K. (2000). Various abiotic stresses rapidly activate Arabidopsis MAP kinases ATMPK4 and ATMPK6. Plant J. **24:** 655–665.

Ishikawa, M., Soyano, T., Nishihama, R., and Machida, Y. (2002). The NPK1 mitogen-activated protein kinase kinase kinase contains a functional nuclear localization signal at the binding site for the NACK1 kinesin-like protein. Plant J. **32:** 789–798.

Ketelaar, T., Allwood, E.G., and Hussey, P.J. (2007). Actin organization and root hair development are disrupted by ethanol-induced overexpression of Arabidopsis actin interacting protein 1 (AIP1). New Phytol. **174:** 57–62.

Kinoshita, E., Kinoshita-Kikuta, E., and Koike, T. (2009). Separation and detection of large phosphoproteins using Phos-tag SDS-PAGE. Nat. Protoc. **4:** 1513–1521.

Kinoshita, E., Kinoshita-Kikuta, E., Takiyama, K., and Koike, T. (2006). Phosphate-binding tag, a new tool to visualize phosphorylated proteins. Mol. Cell. Proteomics **5:** 749–757.

Komis, G., Apostolakos, P., Gaitanaki, C., and Galatis, B. (2004). Hyperosmotically induced accumulation of a phosphorylated p38-like MAPK involved in protoplast volume regulation of plasmolyzed wheat root cells. FEBS Lett. **573:** 168–174.

Komis, G., Apostolakos, P., and Galatis, B. (2002). Hyperosmotic stress induces formation of tubulin macrotubules in root-tip cells of *Triticum turgidum*: Their probable involvement in protoplast volume control. Plant Cell Physiol. **43:** 911–922.

Komis, G., Quader, H., Galatis, B., and Apostolakos, P. (2006). Macrotubule-dependent protoplast volume regulation in plasmolysed root-tip cells of *Triticum turgidum*: Involvement of phospholipase D. New Phytol. **171:** 737–750.

Koushika, S.P. (2008). "JIP"ing along the axon: the complex roles of JIPs in axonal transport. Bioessays **30:** 10–14.

Kovtun, Y., Chiu, W.L., Zeng, W., and Sheen, J. (1998). Suppression of auxin signal transduction by a MAPK cascade in higher plants. Nature. **395:** 716–720.

Kovtun, Y., Chiu, W.L., Tena, G., and Sheen, J. (2000). Functional analysis of oxidative stress-activated mitogen-activated protein kinase cascade in plants. Proc. Natl. Acad. Sci. USA **97:** 2940–2945.

Krysan, P.J., Jester, P.J., Gottwald, J.R., and Sussman, M.R. (2002). An *Arabidopsis* mitogen-activated protein kinase kinase kinase gene family encodes essential positive regulators of cytokinesis. Plant Cell **14:** 1109–1120.

Mao, G., Buschmann, H., Doonan, J.H., and Lloyd, C.W. (2006). The role of MAP65-1 in MT bundling during *Zinnia* tracheary element formation. J. Cell Sci. **119:** 753–758.

Marc, J., Granger, C.L., Brincat, J., Fisher, D.D., Kao, Th., McCubbin, A.G., and Cyr, R.J. (1998). A GFP-MAP4 reporter gene for visualizing cortical microtubule rearrangements in living epidermal cells. Plant Cell **10:** 1927–1940.

Melikant, B., Giuliani, C., Halbmayer-Watzina, S., Limmongkon, A., Heberle-Bors, E., and Wilson, C. (2004). The *Arabidopsis thaliana* MEK AtMKK6 activates the MAP kinase AtMPK13. FEBS Lett. **576:** 5–8.

Menges, M., Dóczi, R., Okrész, L., Morandini, P., Mizzi, L., Soloviev, M., Murray, J.A., and Bögre, L. (2008). Comprehensive gene expression atlas for the *Arabidopsis* MAP kinase signalling pathways. New Phytol. **179:** 643–662.

Mészáros, T., Helfer, A., Hatzimasoura, E., Magyar, Z., Serazetdinova, L., Rios, G., Bardóczy, V., Teige, M., Koncz, C., Peck, S., and Bögre, L. (2006). The Arabidopsis MAP kinase kinase MKK1 participates in defence responses to the bacterial elicitor flagellin. Plant J. **48:** 485–498.

Müller, J., Beck, M., Mettbach, U., Komis, G., Hause, G., Menzel, D.,

and Šamaj, J. (2010). Arabidopsis MPK6 is involved in cell division plane control during early root development, and localizes to the preprophase band, phragmoplast, trans-Golgi network and plasma membrane. Plant J. **61:** 234–248.

Müller, J., Menzel, D., and Šamaj, J. (2007). Cell-type-specific disruption and recovery of the cytoskeleton in *Arabidopsis thaliana* epidermal root cells upon heat shock stress. Protoplasma **230:** 231–242.

Müller, S., Smertenko, A., Wagner, V., Heinrich, M., Hussey, P.J., and Hauser, M.T. (2004). The plant MT-associated protein AtMAP65-3/PLE is essential for cytokinetic phragmoplast function. Curr. Biol. **14:** 412–417.

Nakagami, H., Soukupová, H., Schikora, A., Zárský, V., and Hirt, H. (2006). A mitogen-activated protein kinase kinase kinase mediates reactive oxygen species homeostasis in *Arabidopsis.* J. Biol. Chem. **281:** 38697–38704.

Naoi, K., and Hashimoto, T. (2004). A semidominant mutation in an *Arabidopsis* mitogen-activated protein kinase phosphatase-like gene compromises cortical microtubule organization. Plant Cell **16:** 1841–1853.

Nishihama, R., Ishikawa, M., Araki, S., Soyano, T., Asada, T., and Machida, Y. (2001). The NPK1 mitogen-activated protein kinase kinase kinase is a regulator of cell-plate formation in plant cytokinesis. Genes Dev. **15:** 352–363.

Nishihama, R., and Machida, Y. (2000). The MAP kinase cascade that includes MAPKKK-related protein kinase NPK1 controls a mitotic process in plant cells. Results Probl. Cell Differ. **27:** 119–130.

Nishihama, R., and Machida, Y. (2001). Expansion of the phragmoplast during plant cytokinesis: A MAPK pathway may MAP it out. Curr. Opin. Plant Biol. **4:** 507–512.

Nishihama, R., Soyano, T., Ishikawa, M., Araki, S., Tanaka, H., Asada, T., Irie, K., Ito, M., Terada, M., Banno, H., Yamazaki, Y., and Machida, Y. (2002). Expansion of the cell plate in plant cytokinesis requires a kinesin-like protein/MAPKKK complex. Cell **109:** 87–99.

Oh, H., and Irvine, K.D. (2008). In vivo regulation of Yorkie phosphorylation and localization. Development **135:** 1081–1088.

Panteris E., Komis G., Adamakis I-D.S., Šamaj J., and Bosabalidis A.M. (2010). MAP65 in tubulin/colchicine paracrystals of *Vigna sinensis* root cells: Possible role in the assembly and stabilization of atypical tubulin polymers. Cytoskeleton **67:** 152–160.

Parker, C.G., Hunt, J., Diener, K., McGinley, M., Soriano, B., Keesler, G.A., Bray, J., Yao, Z., Wang, X.S., Kohno, T., and Lichenstein, H.S. (1998). Identification of stathmin as a novel substrate for p38 delta. Biochem. Biophys. Res. Commun. **249:** 791–796.

Petersen, M., et al. (2000). Arabidopsis map kinase 4 negatively regulates systemic acquired resistance. Cell **103:** 1111–1120.

Reszka, A.A., Bulinski, J.C., Krebs, E.G., and Fischer, E.H. (1997). Mitogen-activated protein kinase/extracellular signal-regulated kinase 2 regulates cytoskeletal organization and chemotaxis via catalytic and microtubule-specific interactions. Mol. Biol. Cell **8:** 1219–1232.

Reszka, A.A., Seger, R., Diltz, C.D., Krebs, E.G., and Fischer, E.H. (1995). Association of mitogen-activated protein kinase with the microtubule cytoskeleton. Proc. Natl. Acad. Sci. USA **92:** 8881–8885.

Sakai, T., et al. (2008). Armadillo repeat-containing kinesins and a NIMA-related kinase are required for epidermal-cell morphogenesis in Arabidopsis. Plant J. **53:** 157–171.

Šamaj, J., Baluska, F., and Hirt, H. (2004). From signal to cell polarity: mitogen-activated protein kinases as sensors and effectors of cytoskeleton dynamicity. J. Exp. Bot. **55:** 189–198.

Sangwan, V., Orvar, B.L., Beyerly, J., Hirt, H., and Dhindsa, R.S. (2002). Opposite changes in membrane fluidity mimic cold and heat stress activation of distinct plant MAP kinase pathways. Plant J. **31:** 629–638.

Sasabe, M., and Machida, Y. (2006). MAP65: A bridge linking a MAP kinase to MT turnover. Curr. Opin. Plant Biol. **9:** 563–570.

Sasabe, M., Soyano, T., Takahashi, Y., Sonobe, S., Igarashi, H., Itoh, T.J., Hidaka, M., and Machida, Y. (2006). Phosphorylation of NtMAP65-1 by a MAP kinase down-regulates its activity of MT bundling and stimulates progression of cytokinesis of tobacco cells. Genes Dev. **20:** 1004–1014.

Sauer, M., Paciorek, T., Benková, E., and Friml, J. (2006). Immunocytochemical techniques for whole-mount in situ protein localization in plants. Nat. Protoc. **1:** 98–103.

Sedbrook, J.C. (2004). MAPs in plant cells: Delineating microtubule growth dynamics and organization. Curr. Opin. Plant Biol. **7:** 632–640.

Sedbrook, J.C., and Kaloriti, D. (2008). Microtubules, MAPs and plant directional cell expansion. Trends Plant Sci. **13:** 303–310.

Sieberer, B.J., Ketelaar, T., Esseling, J.J., and Emons, A.M. (2005). Microtubules guide root hair tip growth. New Phytol. **167:** 711–719.

Sikkema, A.H., Diks, S.H., den Dunnen, W.F., Elst, A., Scherpen, F.J., Hoving, E.W., Ruijtenbeek, R., Boender, P.J., de Wijn, R., Kamps, W.A., Peppelenbosch, M.P., and de Bont, E.S. (2009). Kinome profiling in pediatric brain tumors as a new approach for target discovery. Cancer Res. **69:** 5987–5995.

Smertenko, A.P., Chang, H.Y., Sonobe, S., Fenyk, S.I., Weingartner, M., Bögre, L., and Hussey, P.J. (2006). Control of the AtMAP65-1 interaction with MTs through the cell cycle. J. Cell Sci. **119:** 3227–3237.

Smertenko, A.P., Chang, H.Y., Wagner, V., Kaloriti, D., Fenyk, S., Sonobe, S., Lloyd, C., Hauser, M.T., and Hussey, P.J. (2004). The *Arabidopsis* MT-associated protein AtMAP65-1: Molecular analysis of its MT bundling activity. Plant Cell **16:** 2035–2047.

Smertenko, A.P., Kaloriti, D., Chang, H.Y., Fiserova, J., Opatrny, Z., and Hussey, P.J. (2008). The C-terminal variable region specifies the dynamic properties of *Arabidopsis* microtubule-associated protein MAP65 isotypes. Plant Cell **20:** 3346–3358.

Smith, L.G. (2001). Plant cell division: Building walls in the right places. Nat. Rev. Mol. Cell Biol. **2:** 33–39.

Soyano, T., Ishikawa, M., Nishihama, R., Araki, S., Ito, M., Ito, M., and Machida, Y. (2002). Control of plant cytokinesis by an NPK1-mediated mitogen-activated protein kinase cascade. Philos. Trans. R. Soc. Lond. B Biol. Sci. **357:** 767–775.

Soyano, T., Nishihama, R., Morikiyo, K., Ishikawa, M., and Machida, Y. (2003). NQK1/NtMEK1 is a MAPKK that acts in the NPK1 MAPKKK-mediated MAPK cascade and is required for plant cytokinesis. Genes Dev. **17:** 1055–1067.

Strompen, G., El Kasmi, F., Richter, S., Lukowitz, W., Assaad, F.F., Jürgens, G., and Mayer, U. (2002). The *Arabidopsis* HINKEL gene encodes a kinesin-related protein involved in cytokinesis and is expressed in a cell cycle-dependent manner. Curr. Biol. **12:** 153–158.

Su, S.H., Suarez-Rodriguez, M.C., and Krysan, P. (2007). Genetic interaction and phenotypic analysis of the Arabidopsis MAP kinase pathway mutations mekk1 and mpk4 suggests signaling pathway complexity. FEBS Lett. **581:** 3171–3177.

Suarez-Rodriguez, M.C., Adams-Phillips, L., Liu, Y., Wang, H., Su, S.H., Jester, P.J., Zhang, S., Bent, A.F., and Krysan, P.J. (2007). MEKK1 is required for flg22-induced MPK4 activation in Arabidopsis plants. Plant Physiol. **143:** 661–669.

Sugimoto, K., Himmelspach, R., Williamson, R.E., and Wasteneys, G.O. (2003). Mutation or drug-dependent microtubule disruption causes radial swelling without altering parallel cellulose microfibril deposition in *Arabidopsis* root cells. Plant Cell **15:** 1414–1429.

Sugimoto, K., Williamson, R.E., and Wasteneys, G.O. (2001). Wall architecture in the cellulose-deficient rsw1 mutant of *Arabidopsis*

thaliana: Microfibrils but not microtubules lose their transverse alignment before microfibrils become unrecognizable in the mitotic and elongation zones of roots. Protoplasma **215:** 172–183.

Takahashi, Y., Soyano, T., Sasabe, M., and Machida, Y. (2004). A MAP kinase cascade that controls plant cytokinesis. J. Biochem. **136:** 127–132.

Tanaka, H., Ishikawa, M., Kitamura, S., Takahashi, Y., Soyano, T., Machida, C., and Machida, Y. (2004). The AtNACK1/HINKEL and STUD/TETRASPORE/AtNACK2 genes, which encode functionally redundant kinesins, are essential for cytokinesis in *Arabidopsis.* Genes Cells **9:** 1199–1211.

Topping, J.F., Agyeman, F., Henricot, B., and Lindsey, K. (1994). Identification of molecular markers of embryogenesis in *Arabidopsis thaliana* by promoter trapping. Plant J. **5:** 895–903.

Van Damme, D., Van Poucke, K., Boutant, E., Ritzenthaler, C., Inzé, D., and Geelen, D. (2004). In vivo dynamics and differential MT-binding activities of MAP65 proteins. Plant Physiol. **136:** 3956–3967.

Walia, A., Lee, J.S., Wasteneys, G., and Ellis, B. (2009). Arabidopsis mitogen-activated protein kinase MPK18 mediates cortical microtubule functions in plant cells. Plant J. **59:** 565–575.

Wasteneys, G.O. (2002). Microtubule organization in the green kingdom: Chaos or self-order? J. Cell Sci. **115:** 1345–1354.

Wasteneys, G.O., and Ambrose, J.C. (2009). Spatial organization of plant cortical microtubules: Close encounters of the 2D kind. Trends Cell Biol. **19:** 62–71.

Whittington, A.T., Vugrek, O., Wei, K.J., Hasenbein, N.G., Sugimoto, K., Rashbrooke, M.C., and Wasteneys, G.O. (2001). MOR1 is essential for organizing cortical microtubules in plants. Nature **411:** 610–613.

Wiedemeier, A.M., Judy-March, J.E., Hocart, C.H., Wasteneys, G.O., Williamson, R.E., and Baskin, T.I. (2002). Mutant alleles of Arabidopsis RADIALLY SWOLLEN 4 and 7 reduce growth anisotropy without altering the transverse orientation of cortical microtubules or cellulose microfibrils. Development **129:** 4821–4830.

Yang, C.Y., Spielman, M., Coles, J.P., Li, Y., Ghelani, S., Bourdon, V., Brown, R.C., Lemmon, B.E., Scott, R.J., and Dickinson, H.G. (2003). TETRASPORE encodes a kinesin required for male meiotic cytokinesis in *Arabidopsis.* Plant J. **34:** 229–240.

Yang, G., Gao, P., Zhang, H., Huang, S., and Zheng, Z.L. (2007). A mutation in MRH2 kinesin enhances the root hair tip growth defect caused by constitutively activated ROP2 small GTPase in Arabidopsis. PLoS One **2:** e1074.